photonics

MDPI

Article

The Optimization of a Segmented Cladding Fiber via the Response Surface Methodology Approach for a Large Mode Area

Marzieh Pournoury [1,*], Ali Zamiri [2], Marjan Ghasemi [3] and Donghyun Kim [1]

[1] School of Electrical and Electronic Engineering, Yonsei University, Seoul 03722, Republic of Korea; kimd@yonse.ac.kr
[2] School of Mechanical Engineering, Korea University, Seoul 03722, Republic of Korea; alizamiri@korea.ac.kr
[3] Department of Physics, Yonsei University, Seoul 03722, Republic of Korea; m.g480@yonse.ac.kr
* Correspondence: marziehpn@yonsei.ac.kr

Abstract: In this work, we have proposed and optimized a segmented cladding fiber (SCF) with a large mode area (LMA) consisting of a uniform core and a double cladding. The outer cladding of the SCF consisted of a periodic alternation of high- and low-refractive-index segments, while the inner cladding consisted of a resonant layer of rods surrounded by high-refractive-index rings. The three geometrical parameters chosen as design variables were the (a) doped rod refractive index differences, (b) refractive index differences of rings, and (c) ring thickness. Using the Box–Behnken approach, we selected thirteen different design cases and modeled them numerically using the finite element method (FEM). In order to optimize the features of the proposed fiber, such as the effective mode area (EMA), we applied response surface methodology (RSM). The EMA of the optimal SCF was significantly improved and markedly enlarged to about 706 μm^2 at a wavelength of 1.550 μm. Different properties of the optimized double-cladding octo-wing SCF (DC-OW-SCF), such as confinement losses in the core mode and the first higher-order mode, were studied. The DC-OW-SCF offers the advantages of feasibility in fabrication using the powder-in-tube (PIT) method and provides the possibility of utilization in compact amplifier devices and high-power fiber lasers.

Keywords: fiber optics; fiber design and fabrication; fiber laser

Citation: Pournoury, M.; Zamiri, A.; Ghasemi, M.; Kim, D. The Optimization of a Segmented Cladding Fiber via the Response Surface Methodology Approach for a Large Mode Area. *Photonics* **2023**, *10*, 935. https://doi.org/10.3390/photonics10080935

Received: 14 June 2023
Revised: 22 July 2023
Accepted: 26 July 2023
Published: 16 August 2023

1. Introduction

Over the last decades, fiber lasers have attracted much attention as coherent light sources because of their high energy efficiency, compact structures and good optical quality [1–3]. However, the nonlinear optical effect is the most important factor that limits the output power in the power scaling of fiber lasers [4,5]. An effective method of suppressing the nonlinear effects in high-power fiber lasers is to use fibers with LMAs. For a large EMA, the core area must be increased, resulting in refractive index reduction of the core to satisfy the high-power fiber laser single-mode (SM) requirements. The low refractive index of the core needs to be dispersed evenly over the entire core for SM operation. This can cause multiple problems in the manufacturing of optical fibers, making them susceptible to mechanical bending. In studies in several publications, special fibers, such as holey fibers [6–8], leaky channel fibers [9], photonic crystal fibers (PCFs) [10–13] and step-index fibers, have been manufactured to meet LMA and SM standards [14–16]. However, even in the most cutting-edge facilities, these fiber designs were often too complicated for mass production.

SCFs have demonstrated strong potential to concurrently meet SM and LMA requirements in a manner comparable with that of PCFs [17–20]. These fibers feature cores with a high refractive index and cladding with periodic high- and low-refractive-index segments in the azimuthal direction. SCFs, in contrast to PCFs, have no air holes and offer longitudinal uniformity along the entire length of each fiber. With careful design, the FM of an

SCF can have a low leakage loss while providing high losses to all HOMs. Since all the HOMs in SCFs have high leakage losses, they are effectively stripped off, and SM operation is maintained throughout a wide spectrum range of wavelengths [21]. These characteristics of SCFs have made them suitable for applications in high-power fiber lasers, mid-infrared sensing, dense wavelength division multiplexing and fiber amplifiers [9,10,22,23].

Previously, SCFs have been fabricated using materials such as poly (methyl methacrylate) [24–26] and other types of polymer composites [27]. Silica-based glass SCF fabrication with four segments, in which the interfaces of segments with undoped and doped material bubbles have been generated, has been reported [28]. A hexagonal-wing SCF fabricated with silica by applying the PIT technique [19] with alumina and silica powder has also been reported. Since the previously reported [19] hexagonal-wing SCF had nonidentical segments, its performance was not reliable under bending conditions.

The proposed DC-OW-SCF contains a homogenous solid core, cladding with eight identical segments and a circular core area filled with doped silica (n_1). The inner cladding of the DC-OW-SCF consists of a resonant doped rod layer enclosed in high-refractive-index rings (n_3), while the outer cladding is formed of high- and low-refractive-index materials in the circumferential direction. The SM operation could be assured with a large EMA, approximately 706 m^2, by utilizing the resonant layer as the inner cladding. It is possible to produce DC-OW-SCFs using the stacking and drawing method, which would solve the limitations of conventional chemical vapors [19,29,30]. The extremely large EMA achieved for the optimized DC-OW-SCF, which has the advantage of feasibility of fabrication based on the PIT method, is expected to suppress nonlinear optical effects for high-power fiber laser applications. Unlike previous reported SCFs with hexagonal wings [19], since the proposed DC-OW-SCF has a uniform core with identical high- and low-refractive-index segment geometry, it has demonstrated bend-resistant performance.

We performed a numerical analysis of the proposed DC-OW-SCF's performance. To evaluate the confinement loss and EMA, we used the FEM with COMSOL commercial software. The confinement losses of the LP_{01} mode and all of the HOMs played significant roles in the SCF's performance; therefore, we have thoroughly investigated the effects of physical parameters on losses in the DC-OW-SCF. We concentrated on the fundamental concepts of SCFs: how physical characteristics such as (a) ring thickness, t; (b) refractive index differences of doped rods, Δn; and (c) refractive index differences of rings, Δn_r, affect the losses of LP_{01} and HOMs. The impacts of the physical parameters of the DC-OW-SCF were investigated in order to achieve a larger EMA for effective SM operation over a wide wavelength range. Furthermore, this fiber is expected to suppress the effects of optical nonlinearity for application in high-power fiber lasers. The FEM simulations were conducted to achieve optimal EMA values of LP_{01} with a maximized confinement loss of the LP_{11} mode for better suppression. Considering the three mentioned SCF parameters, we were able to optimize the EMA using the RSM optimization algorithm. The methodology of the design of experiment (DOE) was used to decrease case numbers [31]. We applied the Box–Behnken model, in which 13 different cases were considered for FEM simulation, as in this DOE. The proposed design of the DC-OW-SCF, shown in Figure 1, ensures SM operation and a large EMA of about 706 μm^2 at 1.550 μm.

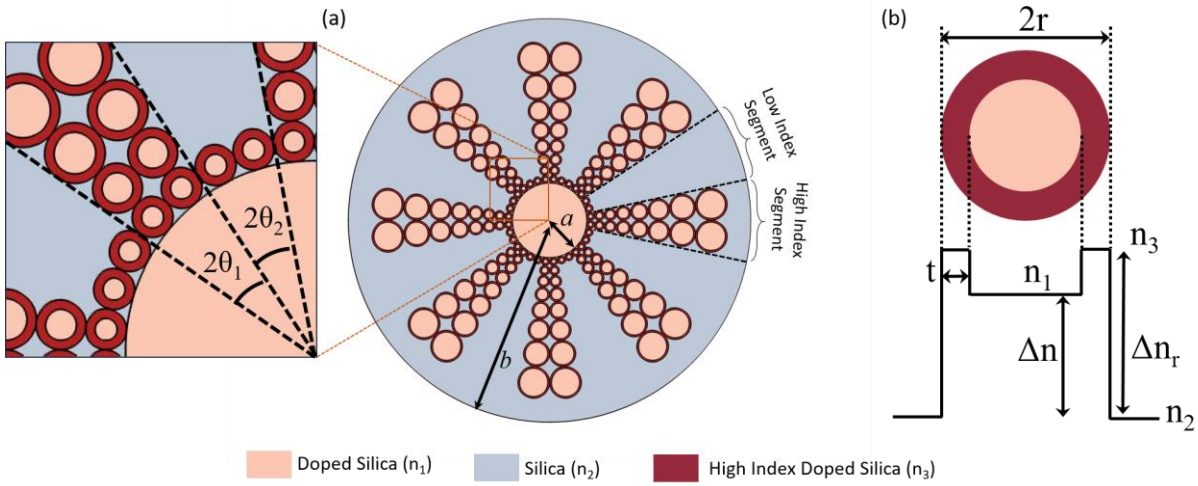

Figure 1. (**a**) Cross-section design of the proposed silica DC-OW-SCF: φ is the orientation of the bending angle, and *a* and *b* are the core and cladding radii, respectively. The magnified cross-section in (**a**) represents the doped silica (n_1), undoped silica (n_2) and high-index doped silica (n_3), with angular widths spanning $2\theta_1$ and $2\theta_2$, respectively. (**b**) Structural parameters of rods with high-index rings: 2*r*, *t*, Δn_r and Δn.

2. Fiber Structure and Numerical Method

2.1. Structural Parameters in the Proposed SCF

In Figure 1a, a cutting plane through the DC-OW-SCF's cross-section geometry is illustrated. The outer cladding is made up of segments with alternating high and low refractive indices that have radii of *b*, while the inner cladding is a resonant layer of doped rods encircled in high-refractive-index rings. In the expanded cross-sectional view of Figure 1a, both the low- and high-index segments, $2\theta_1$ and $2\theta_2$, have angular widths spanning 22.5°. In the FEM simulations, a 5 µm cylindrical PML layer and a refractive index of n_1 were chosen for the area around the outer cladding. The segmentation period (Λ) and duty cycle (γ) were equal to 0.5 and 45, respectively. Figure 1b schematically shows the structural characteristics of the rods with high-index rings; the rod diameter, 2r; the refractive index difference of the doped rods, Δn; the ring thickness, t; and the refractive index difference of the rings, Δn_r. Across the fiber domain and the PML region, structured and unstructured meshes, respectively, were applied. In total, 92814 grid elements and 12185 boundary elements were generated for the entire computational domain.

2.2. Analysis Method

The EMA and leakage loss of the DC-OW-SCF were simulated using a FEM solver (fully vectorial) [32–36]. The real parts of the guided modes were calculated using Maxwell's Equation (1). We applied a PML boundary condition to calculate the complex effective indices: ε_r and μ_r are the electric constant and relative permeability, respectively; k_0 is the wave number in free space; σ is the electric conductivity; and ω is the angular frequency.

$$\nabla \times \left(\mu_r^{-1} \nabla \times \vec{E}\right) - k_0^2 \left(\varepsilon_r - j\frac{\sigma}{\omega \varepsilon_0}\right) \cdot \vec{E} = 0 \quad (1)$$

E_t is the guided-mode transverse electric field and was used to compute the EMA, which was measured in μm^2 according to Equation (2) [32]:

$$A_{eff} = \frac{\left(\iint |E_t|^2 dxdy\right)^2}{\iint |E_t|^4 dxdy} \quad (2)$$

Since we applied PML regions in the simulations, the propagation constant became complex, with both imaginary and real parts. The confinement loss was expressed in dB/m and could be calculated using the imaginary part of the guided-mode effective index [29]:

$$L_c = (20/\ln 10)k_0 \mathrm{Im}\left[n_{eff}\right] \quad (3)$$

Considering the geometrically exact beam theory (GEBT) [37] along with the conformal mapping technique, we calculated the profile of a refractive index of a corresponding straight SCF to determine its bending properties [37]. In the GEBT method, the sources that make changes to a refractive index of a bent SCF are assumed to be geometric and stress effects. In order to consider the geometrical influence generated by the difference in the length of the optical path, followed by the light, we used the conformal mapping technique to map the bent fiber to an equivalent straight SCF [37]:

$$n_{bent} = n_{straight}\left(1 + \frac{\vec{x}\cos\varphi + \vec{y}\sin\varphi}{\rho * R}\right) \quad (4)$$

where ρ is the elasto-optic factor, φ is the bending azimuth angle, R is the bend radius and $n_{straight}$ is the unbent SCF index profile. The bending orientation used in the computation of the bending loss is the OA shown in Figure 1a.

2.3. SM Operation Criteria

Since SM operation in SCFs is based on the leaky structure of the fibers, confinement loss plays an important role in defining their performance. The maximum FM confinement loss is considered to be 0.1 dB/m, while the minimum HOM confinement loss should be 1 dB/m for an SM operation [38,39]. By modifying the geometrical parameters of the DC-OW-SCF and investigating their impacts on confinement loss, the parameters were optimized for SM operation.

3. Optimization Method

The flowchart shown in Figure 2 demonstrates the optimization procedure applied in this paper. In the first step, design variables and corresponding objective functions were selected. Afterward, the DOE approach was applied and several cases were sampled. Subsequently, the objective function values for each designed case were computed with the FEM approach. The obtained objective functions were applied to find the optimal geometrical parameters. The optimization procedure was carried out repeatedly until the ideal conditions were reached.

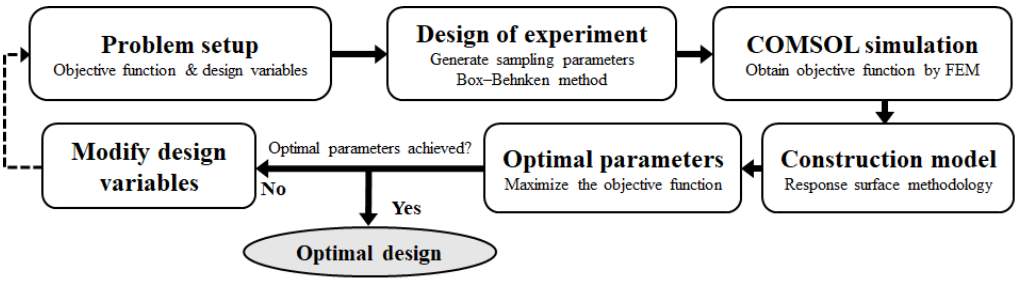

Figure 2. Flowchart diagram for the optimal DC-OW-SCF case. Since the LP_{11} mode needed to be stripped off effectively in order to maintain the SM operation, LP_{11} confinement loss was chosen to be maximized as the second objective function.

3.1. Design Variables and Objective Function

In the optimization procedure of the DC-OW-SCFs, three physical and geometrical parameters were selected: Δn_r, Δn and t. These parameters have significant roles in SCF performance, maximizing the EMA. Other physical and geometrical parameters were

defined as a 10 μm core radius (a), a 1.550 μm wavelength (λ), a 45° Λ value and a γ value of 0.5. The summarized upper and lower bounds of each design variable, defined in Table 1, were chosen based on parametric studies. The EMA was calculated to be maximized as the objective function.

Table 1. Lists of the lower and upper bounds for the design variables.

Design Variable	Lower Bound	Upper Bound
Ring Thickness, μm (t)	0.45	0.7
Doped Rod Refractive Index Difference (Δn)	0.003	0.0036
Refractive Index Differences of Rings (Δn_r)	0.0055	0.0065

In order to reduce the number of experiments, the DOE methodology was applied, taking a statistical approach into account [40]. In the DOE methodology, the procedure of producing samples continuously changes not to only improve information quality but also to exclude unnecessary statistical information, which will result in acceptable source information for an accurate estimation of parameters. There are several DOE models that would have been viable to reduce the required trial. In the current study, the Box–Behnken method, in which three levels of each factor are required [41], was selected. The Box–Behnken method is a nearly rotatable quadratic DOE model in which the number of generated samples (n) is calculated as n = 2m (m − 1) + c; m is the number of central points [31]. In the present optimization study, a total of 13 sampled cases were studied for our numerical FEM simulations. Table 2 summarizes these 13 differently designed cases.

Table 2. Cases designed with the Box–Behnken approach.

Case	Ring Thickness, μm (t)	Refractive Index Differences of Doped Rods (Δn)	Refractive Index Differences of Rings (Δn_r)	Confinement Loss, LP_{11}, dB/m	EMA, μm^2
1	0.450	0.0030	0.0060	4.42	624
2	0.700	0.0033	0.0055	6.64	588
3	0.450	0.0036	0.0060	5.49	481
4	0.450	0.0033	0.0065	2.88	603
5	0.575	0.0030	0.0055	5.74	631
6	0.575	0.0033	0.0060	3.78	614
7	0.700	0.0033	0.0065	1.01	807
8	0.575	0.0030	0.0065	0.911	821
9	0.450	0.0033	0.0055	9.09	491
10	0.575	0.0036	0.0065	2.46	601
11	0.700	0.0036	0.0060	2.00	678
12	0.575	0.0036	0.0055	8.24	471
13	0.700	0.0030	0.0060	1.50	830

3.2. Response Surface Methodology (RSM)

After we performed the numerical simulation for the design cases generated with the Box–Behnken method, the correlations between the computed responses and the design variables needed to be defined with a proper technique. We used RSM optimization [42] to find the optimal geometrical and physical parameters of the DC-OW-SCF in order to maximize the EMA. RSM is very robust and flexible in choosing the proper estimation to relate design variables and response surfaces by applying a second-order model:

$$y = k_0 + \sum_{i=1}^{m} k_i x_i + \sum_{i=1}^{m} k_{ii} x_i^2 + \sum_{i=1}^{m-1} \sum_{j=2}^{m} k_{ij} x_i x_j \quad (5)$$

where y is the objective function, x_i is the ith design variable and k is the unknown coefficient. As a result, we could calculate the optimal point at which the EMA would be maximized.

4. Results and Discussion

Figure 3a,b compare the distributions of modal intensity and the electrical fields as functions of the radial position along the x direction for 13 different cases created using the Box–Behnken approach (see Table 2). It should be noted that the structural parameters of all 13 designed cases were as follows: radii of the core and cladding equal to 10 µm and 62.5 µm, respectively, at λ = 1.55 µm. The impacts of different values of the design optimizations, such as t, Δn and Δn_r, on the electric field distribution area and intensity are clearly shown in Figure 3a,b. From Figure 3a, it is obvious that the larger area of the SCF is covered with the LP_{01} mode around the core region, defined by the light blue color for the cases with thicker rings, smaller refractive index differences of doped rods and larger refractive index differences of rings. In Figure 3b, the electrical field distribution is shown to be less extended in the x direction for cases with thinner rings, larger refractive index differences of doped rods and smaller refractive index differences of rings. Increasing the thicknesses and refractive index differences of the rings in the inner cladding region increased the difference between the core and cladding boundary indices, which could have increased the light confinement in the core and enlarged the mode area of LP_{01}. For the rings located in the high-index segments of the outer cladding, increasing the ring thickness caused the SCF to demonstrate effective SM operation, considering the high-power laser requirements for FM and first HOM limitations.

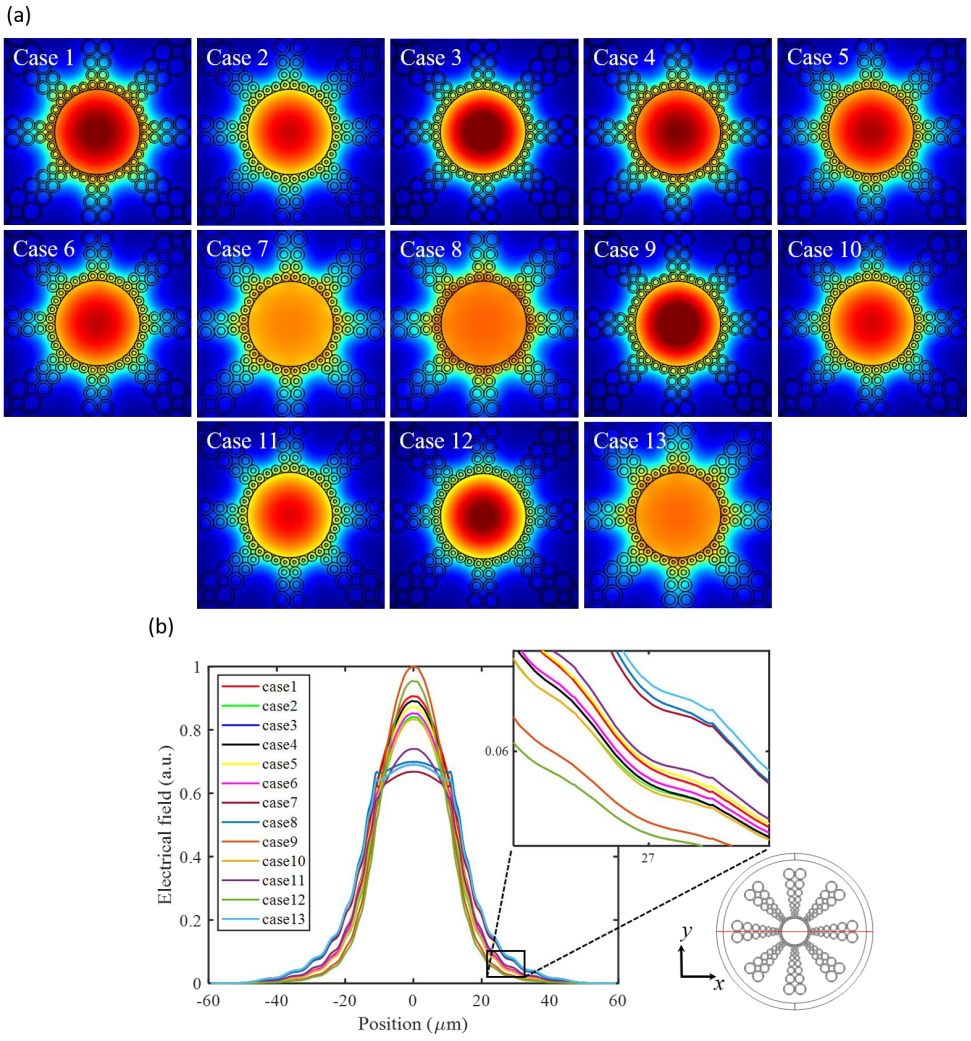

Figure 3. (**a**) Modal intensity and (**b**) electrical field distribution of FM as a function of radial position along the x direction for various cases, based on the Box–Behnken approach. This enlarged electric field view shows the distributions of 13 cases in more detail.

To illustrate the impact of each of the design variables on the objective functions more precisely, in Figure 4a–c, we have plotted the EMAs and the confinement losses of the LP_{01} and LP_{11} modes for all 13 cases. As depicted in Figure 4a, cases 7, 8 and 13 had the highest EMAs, with values above 800 μm^2, and for cases 3, 9 and 12, the EMAs were the lowest, with values below 500 μm^2. In Figure 4b, the confinement losses of the LP_{11} mode for those 13 cases are shown. For cases 7, 8 and 13, with EMAs above 800 μm^2, the LP_{11} mode hardly satisfied the requirement of SM operation, considering the high-power laser limitations of the first HOM. Among all the cases designed with the Box–Behnken method, the one that best met the criteria of effective SM operation for high-power laser application was case 11, which had the largest EMA, of about 678 μm^2, and a confinement LP_{11} loss of more than 1dB/m. It should be noted that as shown in Figure 4c, the LP_{01} mode satisfies the requirements of SM operation for high-power lasers well, with values below 0.1 for all 13 cases. LP_{01} confinement loss was in the order of 10^{-3} and sufficiently lower than 0.1 for all cases as well.

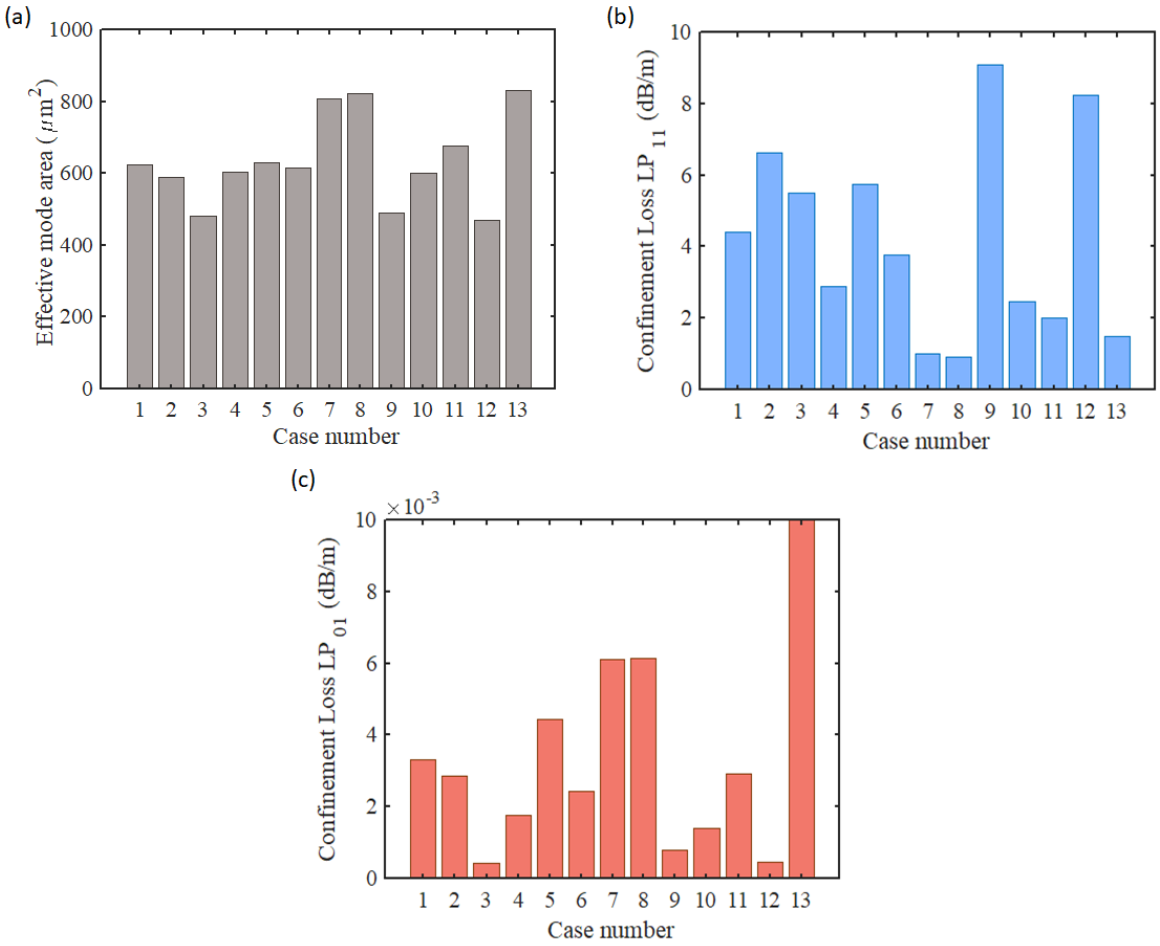

Figure 4. (**a**) EMAs, (**b**) confinement losses for LP_{11} and (**c**) confinement losses of LP_{01} for the 13 different cases designed with the Box–Behnken approach.

Figure 5 shows the effects of the design variables on the EMA. As shown in Figure 5a with the red arrow, the overall EMA enlarged as the ring became thicker.

Moreover, as indicated by the green and blue arrows in Figure 5b,c, while decreased refractive index differences of doped rods made the EMAs larger, larger refractive index differences of rings worked in reverse, increasing the EMAs.

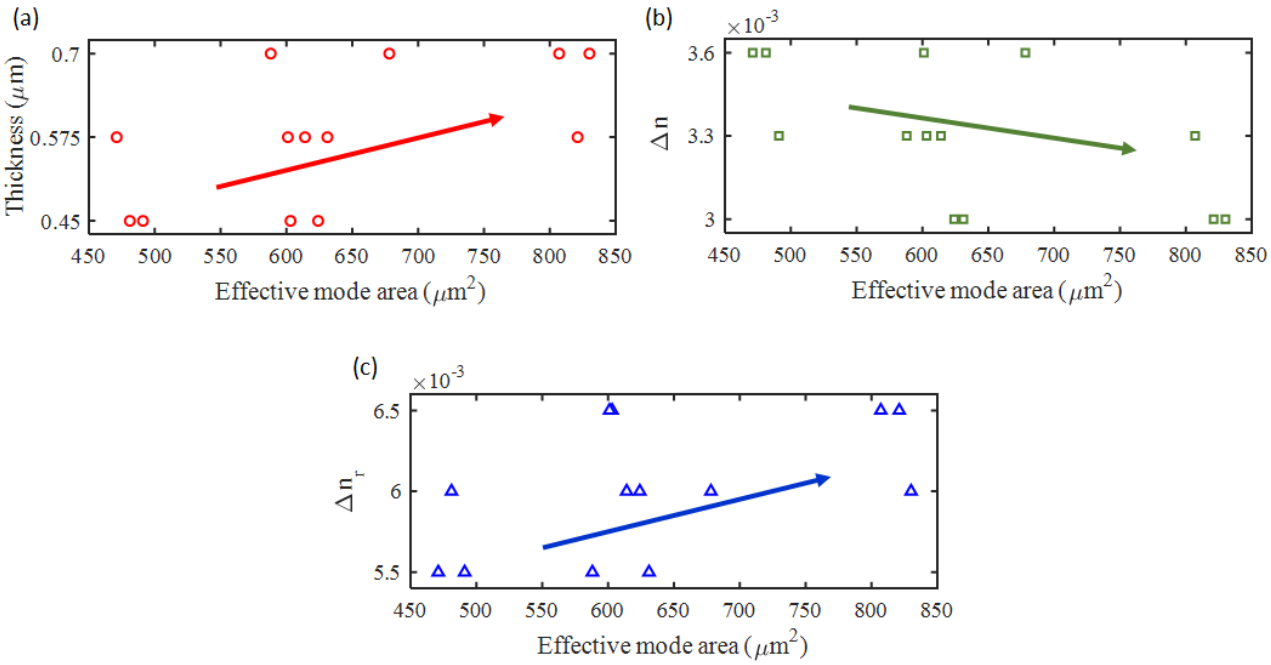

Figure 5. Effects of design variables (**a**) t, (**b**) Δn and (**c**) Δn_r on EMA.

5. Optimization Results

Based on the RSM procedure, we optimized the DC-OW-SCF's performance by varying t, Δn and Δn_r to obtain a larger EMA. Detailed information about the resulting DC-OW-SCF is summarized in Table 3. Based on these results, the ring thickness value was optimized as 0.7 μm and the optimal values of the refractive index differences of the doped rods and rings were 0.003 and 0.0055, respectively.

Table 3. Optimization results based on the RSM approach.

	Opt.
Ring Thickness, μm (t)	0.7
Refractive Index Differences of Doped Rods (Δn)	0.003
Refractive Index Differences of Rings (Δn_r)	0.0055
EMA, μm^2	706
Leakage loss of LP_{11}, dB/m	5.08

As indicated in Table 3, an EMA as large as 706 μm^2 can be achieved with this methodology. The confinement loss of the LP_{11} mode was well above 1 dB/km and satisfied the SM operation criteria for applications in amplifiers and high-power lasers. The difference between the calculated objective function with RSM prediction and the FEM data was about 0.085%, which shows that the optimization method used in this study is accurate.

Figure 6 illustrates the simulation results for the optimized DC-OW-SCF. In Figure 6a,b, the distribution of electric fields for both the LP_{01} and LP_{11} modes as a function of the radial position along the X-axis at a wavelength of 1.550 μm is illustrated. These figures also depict the modal intensities of the FM and the first HOM at a wavelength of 1.550 μm. As illustrated in Figure 6b, LP_{01} was a guided mode in the core region and LP_{11} was well extended in the cladding area. Thus, LP_{11} as a cladding mode could be easily stripped off, consequently providing the SM operation.

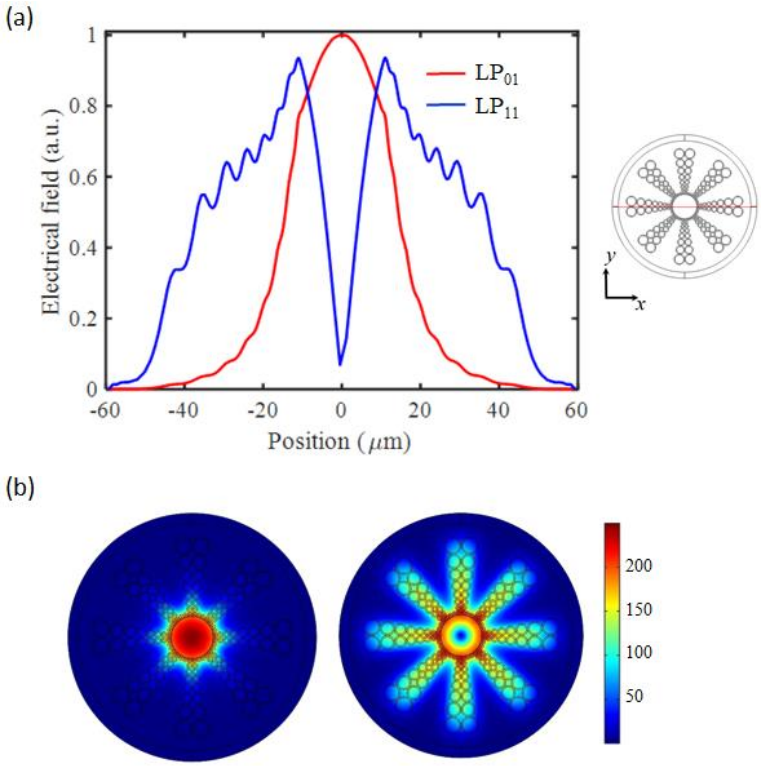

Figure 6. (**a**) Distribution of the electric field as a function of radial position along the X-axis for the LP_{01} and LP_{11} modes. (**b**) Mode field intensity distribution of LP_{01} and LP_{11}.

Figure 7 shows the confinement loss variations of FM and the first HOM at varying wavelengths. According to the results shown in Figure 7, the two most important features of the SCF are the confinement loss of LP_{01}, which is known as absolute loss, and the differential loss of the SCF, defined by the difference between the losses of the LP_{01} and LP_{11} modes. The absolute loss defines how much loss results for an SCF, and the differential loss defines how effective the SCF is in SM operation. Figure 7 shows that the confinement loss of the LP_{11} is significantly larger than that of LP_{01} by more than two orders of magnitude in the wavelength from 1.3 µm to 2 µm.

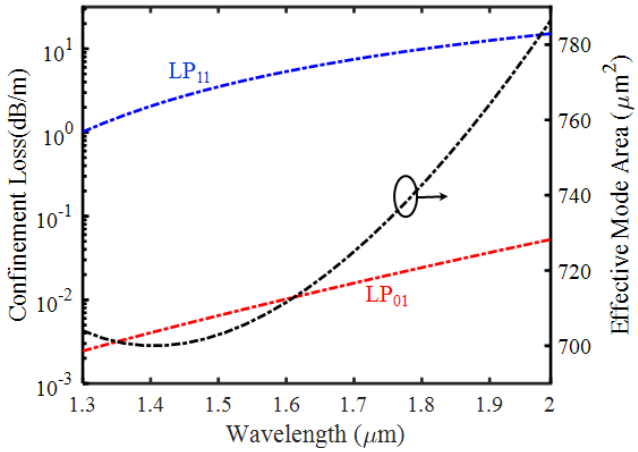

Figure 7. Y-axis on the left: variations of the computed losses of the LP_{01} and LP_{11} modes; Y-axis on the right: EMA of the LP_{01} mode versus wavelength.

As a result, the DC-OW-SCF showed SM behavior along the whole wavelength. At a wavelength of 1.55 µm, the LP_{01} and LP_{11} modes had confinement losses of 0.008 dB/m and 5 dB/m, respectively. In other words, a length of about 4.5 meters of the fiber would

be sufficient for the LP_{11} to be stripped with an extinction ratio of 20 dB. The EMA, as an important parameter of LMA fibers, was calculated with Equation (2), using the FEM for the optimized DC-OW-SCF at different wavelengths. Figure 7 presents an EMA of about 706 μm^2 at the wavelength of 1.55 μm; it increased to above 780 μm^2 at a wavelength of 2 μm.

Since the SCF did not have a circularly symmetric structure, we needed to demonstrate the impact of the bending radius, R, and the bending orientation, φ, for the DC-OW-SCF, as shown in Figure 8a,b. The structural parameters were a core radius of a = 10 μm, a cladding radius of b = 62.5 μm and γ = 0.5 when λ = 1.550 μm. Figure 8a shows that the confinement loss of the LP_{01} mode increased dramatically when the bending radius decreased below 30 cm, and at the larger bending radius, the losses of LP_{01} and LP_{11} demonstrated small changes. Figure 8b illustrates the variation in the bending losses of the core mode and of the first HOM and the EMA of the optimized DC-OW-SCF on φ. It shows that the bending orientation barely had an impact on the performance of the SCF. When a = 10 μm, b = 62.5 μm and γ = 0.5 at the wavelength of λ = 1.550 μm, the confinement loss of LP_{01} was 0.02 dB/km, the loss of LP_{11} was 22 dB/km and the EMA of LP_{01} was about 706 μm^2 along the whole range of the bending orientation. As a result of the constant values of the bending orientation in the whole range of 1 to 30 degrees, it was not necessary to control this orientation.

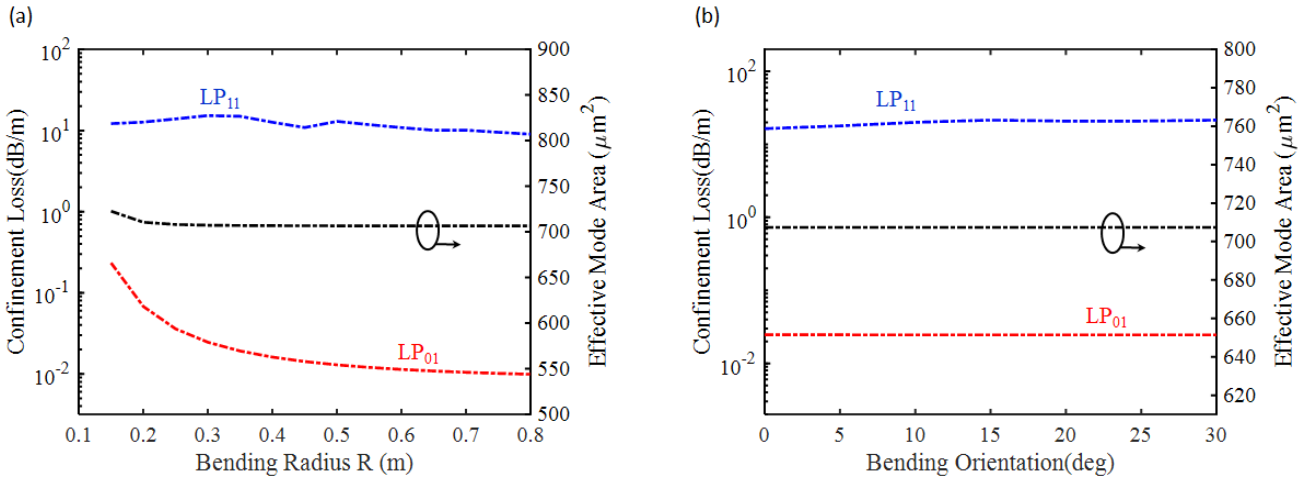

Figure 8. Variations of leakage losses of the LP_{01} and LP_{11} modes and EMAs of the LP_{01} mode versus (**a**) bending radius, R, at φ = 0° and (**b**) bending orientation, φ, at R = 30 cm for the optimized DC-OW-SCF.

Although there has been much attention paid to SCFs due to their large EMAs, there are not many reports on a successful fabrication of SCFs using glass materials. Conventional SCF fabrication has been attempted with low-melting-temperature materials such as poly (methyl methacrylate) [27] and other polymers. Recently, an SCF with a special hexagonal wing design was designed and fabricated [19] with the stack-and-draw technique and the PIT process applied. Since the fabricated SCF with the hexagonal core had nonidentical high and low segments in the cladding [19], it could not provide a reliable performance under bending orientation. The proposed optimized DC-OW-SCF not only has a reliable performance under bending orientation but it also has the advantage of silica-based fabrication feasibility through the previously proposed PIT process, in which the preform can be prepared [19], with different types of rods, out of silica powder and dopant for the other areas with higher refractive indices. After the rods are drawn with proper diameters and dopants, they can be stacked together for the optimized DC-OW-SCF with the cross-section in Figure 1. Finally, after the preparation of the stacked rods, as the final step, the stack will be put in a silica–glass tube. The prepared DC-OW-SCF preform will then be mounted on a drawing tower for the final drawing. The proposed optimized DC-OW-SCF design, which is compatible with silica-based fabrication, can provide a relatively high LMA, at

706 μm^2. Table 4 compares the confinement loss and EMA of the optimized DC-OW-SCF with those of the previous SCF [19]. The extremely large EMA obtained for the optimized DC-OW-SCF with respect to the previous reported SCF [19], along with the SM operation, made it a suitable candidate for applications in high-power fiber lasers in order to overcome nonlinearity issues.

Table 4. Comparison to other reported SCFs when λ = 1.550 μm.

	LP_{01} Loss, dB/m	**LP_{11} Loss, dB/m**	**Mode Area, μm^2**
Ref. [19]	0.49	16.8	231
Proposed	8×10-3	5	706

6. Conclusions

We have proposed a new SCF design with a homogeneous silica core and double cladding, in which the inner cladding is a resonant layer of rods enclosed in high-refractive-index rings and the outer cladding is a circumferential alternation of low- and high-refractive-index segments. A total of 13 cases were studied and sampled by applying the Box–Behnken approach. The confinement losses and EMAs of the 13 different design cases were numerically simulated using the FEM from COMSOL. Considering those 13 study cases, the physical fiber features were optimized by applying RSM to enlarge the EMA. The geometrical SCF parameters for optimization were ring thickness, refractive index differences of doped rods and refractive index differences of rings. We showed that the overall EMAs enlarged as the rings became thicker. Moreover, we demonstrated that while decreasing the refractive index differences of doped rods will make an EMA larger, larger refractive index differences of rings will work in reverse and increase the EMA. In the optimized case, the confinement loss of the LP_{11} mode was shown to be significantly larger than that of the LP_{01} mode, by more than two orders of magnitude. As a result, the DC-OW-SCF demonstrated SM behavior over a wide range of wavelengths. An EMA of about 706 μm^2 at λ = 1.55 μm was achieved for the optimized DC-OW-SCF. At a wavelength of 2 μm, the EMA was increased to above 780 μm^2. The proposed DC-OW-SCF structure can be made using the silica-based fabrication method, and because of its large EMA and excellent SM performance, it has potential for high-performance delivery devices such as high-power lasers.

Author Contributions: Conceptualization, methodology, software, writing—original draft preparation, M.P.; software, M.G.; methodology, A.Z.; review and editing, D.K. All authors have read and agreed to the published version of this manuscript.

Funding: This work was supported by the National Research Foundation of Korea, under Grant NRF-2022R1A4A2000748, and Y-BASE R&E Institute, a Brain Korea 21 four program, Yonsei University.

Institutional Review Board Statement: Not applicable.

Informed Consent Statement: Not applicable.

Data Availability Statement: Data sharing is not applicable to this article.

Conflicts of Interest: The authors declare no conflict of interest.

References

1. Berdine, R.W.; Motes, R.A. *Introduction to High Power Fiber Lasers*, 1st ed.; Directed Energy Professional Society: Albuquerque, NM, USA, 2009.
2. Jauregui, C.; Limpert, J.; Tünnermann, A. High power fiber lasers. *Nat. Photonics* **2013**, *7*, 861–867. [CrossRef]
3. Nilsson, J.; Payne, D.N. High Power Fiber Lasers. *Science* **2011**, *332*, 921–922. [CrossRef] [PubMed]
4. Wen, H.; Zhai, Y.; Lu, B.; Chen, H. Single-Longitudinal Mode Ytterbium-Doped Fiber Laser with Ultra-Narrow Linewidth and High OSNR Using a Double-Ring Passive Subcavity. *Photonics* **2023**, *10*, 500. [CrossRef]
5. Jauregui, C.; Eidam, T.; Otto, H.; Stutzki, F.; Jansen, F.; Limpert, J.; Tünnermann, A. Physical origin of mode instabilities in high-power fiber laser systems. *Opt. Express* **2012**, *20*, 12912–12925. [CrossRef]

6. Hu, D.; Shum, P.; Lu, C.; Yu, X.; Wang, G.; Ren, G. Holey fiber design for single-polarization single-mode guidance. *Appl. Opt.* **2009**, *48*, 4038–4043. [CrossRef]
7. Pournoury, M.; Kim, D. Optimized segmented cladding fiber for extreme large mode area using Latin Hypercube sampling. *Opt. Commun.* **2023**, *542*, 129593.
8. Monro, T.; Richardson, D.; Broderick, N.; Bennett, P. Holey Optical Fibers: An Efficient Modal Model. *J. Lightwave Technol.* **1999**, *17*, 1093–1102. [CrossRef]
9. Jung, C.H.; Cho, H.S.; Han, J.W.; Ashok, N.; Shin, W.J.; Ouh, C.H. Leaky channel fiber design for large mode area high power application at 1 micron. *Fiber Lasers XV Technol. Syst.* **2018**, *10512*, 497–502.
10. Kumar, A.; Saini, T.; Naik, K.; Sinha, R. Large-mode-area single-polarization single-mode photonic crystal fiber: Design and analysis. *Appl. Opt.* **2016**, *55*, 4995–5000. [CrossRef]
11. Knight, J.C. Photonic crystal fibers. *Nature* **2003**, *424*, 847–851. [CrossRef]
12. Limpert, J.; Deguil-Robin, N.; Manek-Hönninger, I.; Salin, F.; Röser, F.; Liem, A.; Schreiber, T.; Nolte, S.; Zellmer, H.; Tünnermann, A.; et al. High-power rod-type photonic crystal fiber laser. *Opt. Express* **2015**, *13*, 1055–1058. [CrossRef]
13. Pinto, A.M.R.; Lopez-Amo, M. All-fiber lasers through photonic crystal fibers. *Nanophotonics* **2013**, *2*, 355–368. [CrossRef]
14. Sidharthan, R.; Lin, D.; Lim, K.J.; Li, H.; Lim, S.H.; Chang, C.J.; Seng, Y.M.; Chua, S.L.; Jung, Y.; Richardson, D.J.; et al. Ultra-low NA step-index large mode area Yb-doped fiber with a germanium doped cladding for high power pulse amplification. *Opt. Lett.* **2020**, *45*, 3828–3831. [CrossRef]
15. Sidharthan, R.; Ji, J.; Lim, K.; Lim, S.; Li, H.; Lua, J.; Zhou, Y.; Tse, C.; Ho, D.; Seng, Y.; et al. Step-index high-absorption Yb-doped large-mode-area fiber with Ge-doped raised cladding. *Opt. Lett.* **2018**, *43*, 5897–5900. [CrossRef]
16. Savović, S.; Kovačević, M.S.; Drljača, B.; Simović, A.; Kuzmanović, L.; Djordjevich, A. Power flow in multimode step-index plastic photonic crystal fibers. *Optik* **2021**, *247*, 167868. [CrossRef]
17. Pournoury, M.; Kim, D. Design and optimization of a double cladding octo-wing segmented cladding fiber using response surface methodology, In Proceedings of the 7th IEEE Electron Devices Technology and Manufacturing Conference (EDTM), Seoul, South Korea, 7–10 March, 2023; pp. 1–3.
18. Babita, H.; Rastogi, V.; Kumar, A. Segmented cladding fiber design for femtosecond laser pulse delivery at 1550-nm and 1064-nm wavelengths. In Proceedings of the 17th Opto-Electronics and Communications Conference, Busan, Republic of Korea, 2–6 July 2012; pp. 359–360.
19. Pournoury, M.; Han, S.-R.; Ghasemi, M.; Lee, H.; Kim, D.; Oh, K. Silica segmented cladding fiber design and its fabrication using a powder-in-tube technique. *J. Light. Technol.* **2021**, *39*, 7251–7258. [CrossRef]
20. Pournoury, M.; Lee, Y.S.; Kim, D.; Oh, K. Granulated Silica Segmented Cladding Fiber for Optical Communication. In Proceedings of the Opto-Electronics and Communications Conference (OECC), Hong Kong, China, 3–7 July 2021.
21. Rastogi, V.; Chiang, K.S. Analysis of the segmented cladding fiber by the radial effective-index method. *J. Opt. Soc. Amer. B* **2004**, *21*, 258–265. [CrossRef]
22. Yang, S.; Zhang, W.; She, Y.; Du, H.; Tu, S. A Large Mode Area Parabolic-Profile Core Fiber with Modified Segmented in Cladding. *Photonics* **2022**, *9*, 783. [CrossRef]
23. Aleshkina, S.S.; Likhachev, M.E.; Lipatov, D.S.; Medvedkov, O.I.; Bobkov, K.K.; Bubnov, M.M.; Guryanov, A.N. 5.5 W monolitic single-mode fiber laser and amplifier operating near 976 nm. *Fiber Lasers XIII Technol. Syst. Appl.* **2016**, *9728*, 265–272.
24. Millo, A.; Naeh, I.; Katzir, A. Single-Mode Segmented Cladding Fibers for the Middle Infrared. *J. Light. Technol.* **2007**, *25*, 2115–2121. [CrossRef]
25. Duan, J.; Teng, C.; Han, K.; Yu, M.; Wu, W.; Zhang, Q.; Chiang, K.S. Fabrication of segmented cladding fiber by bicomponent spinning. *Polym. Eng. Sci.* **2009**, *49*, 1865–1870. [CrossRef]
26. Yeung, A.; Chiang, K.S.; Rastogi, V.; Chu, P.L.; Peng, G.D. Experimental demonstration of single-mode operation of large-core segmented cladding fiber. In Proceedings of the Optical Fiber Communication Conference, Los Angeles, CA, USA, 23–27 February 2004.
27. Yeung, A.; Chu, P.L.; Peng, G.D.; Chiang, K.S.; Liu, Q. Design and fabrication of polymer cross fiber for large-core single-mode operation. *J. Light. Technol.* **2009**, *27*, 101–107. [CrossRef]
28. Hooda, B.; Pal, A.; Rastogi, V.; Sen, R.; Gandhi, J.; Kobelke, J. Segmented cladding fiber fabricated in silica-based glass. *Opt. Eng.* **2015**, *54*, 075103. [CrossRef]
29. Pournoury, M.; Kim, D. Bend-resistant octo-wing silica segmented cladding fiber with high index rings. *Results Phys.* **2022**, *36*, 105423. [CrossRef]
30. Ballato, J.; Snitze, E. Fabrication of fibers with high rare-earth concentrations for Faraday isolator applications. *Appl. Opt.* **1995**, *34*, 6848–6854. [CrossRef]
31. Zamiri, A.; You, S.J.; Chung, J.T. Large Eddy Simulation in the Optimization of Laidback Fan-Shaped Hole Geometry to Enhance Film-Cooling Performance. *Int. J. Heat Mass Transf.* **2020**, *158*, 120014. [CrossRef]
32. Pournoury, M.; Moon, D.S.; Oh, K. Ultra-low loss fiber with segmented-core and depressed inner cladding. In Proceedings of the Asia Communications and Photonics Conference, Hong Kong, China, 19–23 November 2015.
33. Koshiba, M. Optical Waveguide Theory by the Finite Element Method. In *IEICE Transactions on Electronics*; Springer: Dordrecht, The Netherlands, 2014; Volume E97-C, pp. 625–635.

34. Dautov, R.Z.; Karchevskii, E.M. Numerical Modeling of Optical Fibers Using the Finite Element Method and an Exact Non-reflecting Boundary Condition. *Comput. Methods Appl. Math.* **2018**, *18*, 581–601. [CrossRef]
35. Kawano, K.; Kitoh, T. *Finite-Element Methods Introduction to Optical Waveguide Analysis*, 1st ed.; Wiley: New York, NY, USA, 2001; pp. 59–68.
36. Pournoury, M.; Moon, D.S.; Oh, K. Low scattering loss fiber with segmented-core and depressed inner cladding structure. *Opt. Commun.* **2014**, *317*, 13–17. [CrossRef]
37. Velamuri, A.V.; Patel, K.; Sharma, I.; Gupta, S.S.; Gaikwad, S.; Krishnamurthy, P.K. Investigation of Planar and Helical Bend Losses in Single- and Few-Mode Optical Fibers. *J. Lightwave Technol.* **2019**, *37*, 3544–3556. [CrossRef]
38. Guo, Z.; Pei, L.; Ning, T.; Zheng, J.G.; Li, J.; Wang, J. Resonant-ring assisted large mode area segmented cladding fiber with high-index rings in core. *Opt. Commun.* **2021**, *495*, 127049.
39. Dong, L.; Peng, X.; Li, J. Leakage channel optical fibers with large effective area. *J. Opt. Soc. Am. B* **2007**, *24*, 1689–1697. [CrossRef]
40. Fisher, S.R.A. *The Design of Experiments*, 9th ed.; Hafner Publishing Company: New York, NY, USA, 1971.
41. Box, G.E.P.; Behnken, D.W. Some new three level designs for the study of quantitative variables. *J. Technometrics* **1960**, *2*, 455–475. [CrossRef]
42. Myers, R.H.; Montgomery, D.C. *Response Surface Methodology*, 2nd ed.; Wiley: New York, NY, USA, 2002.